Stenoparib, an inhibitor of cellular poly (ADP-ribose) polymerase (PARP), blocks replication of the SARS-CoV-2 human coronavirus *in vitro*.

Nathan E. Stone[a], Sierra A. Jaramillo[a], Ashley N. Jones[a], Adam J. Vazquez[a], Madison Martz[a], Lora M. Versluis[ab], Marlee O. Raniere[ab]., Haley E. Nunnally[a], Katherine E. Zarn[a], Roxanne Nottingham[a], Jason W. Sahl[ab], David M. Wagner[ab], Steen Knudsen[c], Erik W. Settles[ab], Paul S. Keim[ab], Christopher T. French[ab]#.

[a]Pathogen and Microbiome Institute, Northern Arizona University, Flagstaff, AZ 86011-4073

[b]Department of Biological Sciences, Northern Arizona University, Flagstaff, AZ 86011-5640

[c]Allarity Therapeutics, DK-2970 Hørsholm, Denmark

Running Head: Stenoparib inhibits SARS-CoV-2 *in vitro*

#Address correspondence to Christopher T. French, ctfrench@nau.edu

ABSTRACT

By late 2020, the coronavirus disease (COVID-19) pandemic, caused by SARS-CoV-2 has caused tens of millions of infections and over 1 million deaths worldwide. A protective vaccine and more effective therapeutics are urgently needed. We evaluated a new PARP inhibitor, stenoparib, which was recently advanced to Stage II clinical trials for treatment of ovarian cancer, for activity against human respiratory coronaviruses, including SARS-CoV-2, *in vitro*. Stenoparib exhibits dose-dependent suppression of SARS-CoV-2 multiplication and spread in Vero E6 monkey kidney and Calu-3 human lung adenocarcinoma cells. Stenoparib was also

strongly inhibitory to the HCoV-NL63 human seasonal respiratory coronavirus. Compared to
26 remdesivir, which inhibits viral replication downstream of cell entry, stenoparib impedes entry
and post-entry processes as determined by time-of-addition (TOA) experiments. Moreover, a 10
28 μM dosage of stenoparib – below the approximated 25.5 μM half-maximally effective
concentration (EC_{50}), combined with 0.5 μM remdesivir suppressed coronavirus growth by more
30 than 90%, indicating a potentially synergistic effect for this drug combination. Stenoparib as a
standalone or as part of combinatorial therapy with remdesivir should be a valuable addition to
32 the arsenal against COVID-19.

34

Importance

36 New therapeutics are urgently needed in the fight against COVID-19. Repurposing drugs that are either already approved for human use or are in advanced stages of the approval process 38 can facilitate more rapid advances toward this goal. The PARP inhibitor stenoparib may be such a drug, as it is currently in Stage II clinical trials for the treatment of ovarian cancer and its safety 40 and dosage in humans has already been established. Our results indicate that stenoparib possesses strong antiviral activity against SARS-CoV-2 and other coronaviruses *in vitro.* This 42 activity appears to be based on multiple modes of action, where both pre-entry and post-entry viral replication processes are impeded. This may provide a therapeutic advantage over many 44 current options that have a narrower target range. Moreover, our results suggest that stenoparib and remdesivir in combination may be especially potent against coronavirus infection.

46

48 **Introduction**

The novel SARS-CoV-2 coronavirus emerged from Wuhan, China in late 2019, and
50 rapidly spanned the globe in a devastating pandemic (1). The disease, COVID-19, compromises the upper and lower respiratory systems and may affect all people (2). Although in many cases
52 COVID-19 symptoms may be mild, some patients present with pulmonary distress leading to severe lung damage, and treatment options are limited (1, 3-5). Mortality estimates range from
54 0.5% to more than 5% (6). According to the Johns Hopkins COVID Resource Center (7), as of Nov. 10, 2020, over 10 million infections and more than 240,000 deaths have occurred due to
56 COVID-19 in the USA alone, and the pandemic continues (8). A protective vaccine may become available (1, 2), but unless sufficient immunity can be achieved in the population, COVID-19 has
58 the potential to cause morbidity and mortality for years to come. Without a protective vaccine, COVID-19 has largely been controlled through non-pharmaceutical measures such as quarantine,
60 social isolation, and the use of personal protective equipment. Clearly, more efficacious treatments are needed.

62 Individuals who contract COVID-19 are most commonly infected by person-to-person transmission, where inhaled droplets containing infectious virions are seeded into the respiratory
64 tract (1). The virions bind to respiratory epithelium via the affinity of the virus spike (S) complex to the angiotensin converting enzyme 2 (ACE2) receptor (9). A cellular serine protease
66 TMPRSS2 plays a pivotal role in S protein priming (10), which in turn facilitates fusion between the viral and cellular plasma membranes and internalization of the virus-receptor complex by
68 endocytosis. Subsequently, the virus is uncoated and releases its single-stranded RNA genome, which is processed, translated, and replicated in the host cytosol. Copies of the viral genome are
70 packaged into bilayer membrane envelopes, and these new infectious virions are exported from

the cell (11, 12). The SARS-CoV-2 lifecycle is typical of other coronaviruses, including the
72 highly virulent SARS-CoV, the cause of Severe Acquired Respiratory Syndrome (SARS) (9).
Conservation of key steps in the coronavirus viral lifecycles potentially constitutes an 'Achilles
74 Heel' that is broadly susceptible to therapeutic intervention.

Antiviral therapeutics impede interactions between the virus and the host cell. Potential
76 targets include the virus binding to the cellular receptor, viral entry or virus-host membrane
fusion, viral transcription, translation, replication and export. (1). Stenoparib is an
78 investigational, orally-available small molecule that inhibits poly (ADP- ribose) polymerase
(PARP), a key enzyme in DNA repair (13). Stenoparib is unique in that it has dual inhibitory
80 activity against the PARP 1/2 and tankyrase 1/2 enzymes, which are important regulators of the
canonical Wnt/β-catenin checkpoint that is often dysregulated in metastatic breast cancer (14).
82 Until August 2020, stenoparib was known as "2X-121" and previously as "E7449". Recently,
another PARP inhibitor mefuparib (CVL218) was shown to inhibit SARS-CoV-2 *in vitro*.
84 CVL218 suppressed SARS-CoV-2 infection in Vero E6 African Green Monkey cells (15). As
implied by molecular modeling studies, CVL218 and other PARP inhibitors may block viral
86 replication by interfering the viral nucleocapsid (N) protein binding to an RNA template (15).

The practice of repurposing existing drugs for new indications has advantages over
88 developing an entirely new drug (16, 17). There are numerous repurposed drugs in use, including
zidovudine, which was repurposed from the treatment of cancer to treat HIV/AIDS; the epilepsy
90 drug topiramate, which is used to treat obesity; aspirin for analgesia and the prevention of
colorectal cancer, among other examples (16). With repurposing, the risk of failure is lower
92 compared to developing a new drug, because safety trials have already been completed and the *in
vivo* pharmacokinetics have been characterized; thus, cost and time of development are reduced.

94 Moreover, the repurposing endeavor itself may reveal new disease targets and pathways. Altogether, reproposing can produce more rapid and efficient returns (16, 18). Stenoparib is
96 currently in Phase II clinical trials for the treatment of ovarian cancer (14). Based on the recent promising results of the PARP inhibitor CVL218 against SARS-CoV-2 *in vitro* (15), we
98 evaluated the activity of stenoparib against SARS-CoV-2, with an eye toward its use as a treatment for COVID-19.

100

102 **Results**

Stenoparib inhibits the replication of SARS-CoV-2 in Vero E6 cells. Based on the
104 reported antiviral activity of other PARP inhibitors on SARS-CoV-2 *in vitro* (15) we aimed to determine whether stenoparib possessed a similar activity against the virus. Stenoparib was
106 prepared as a solution in dimethylsulfoxide (DMSO) and used to treat Vero E6 cells infected with SARS-CoV-2 (USA-WA1/2020). Vero E6 is a common cell platform for propagating
108 coronaviruses, including SARS-CoV-2 and SARS-CoV (19, 20). At 48 hours (h) after infection, RNA was isolated from cell supernatants, and viral copy number was estimated by reverse-
110 transcription quantitative real-time polymerase chain reaction (RT-qPCR). Viral RNA measurements were compared to untreated cell controls, and to infected cells treated with a
112 cocktail of camostat mesylate and E64d ('C/E'), which are protease inhibitors that impede processing of the virus spike protein and interfere with its entry into the cell (10, 21). In parallel,
114 we assessed potential toxic effects of stenoparib using the lactate dehydrogenase release assay, which indicates cytotoxicity due to cell lysis. As shown in **Fig. 1**, stenoparib demonstrated dose-
116 dependent activity against SARS-CoV-2 at concentrations up to 30 μM with negligible cytotoxicity. The significant 63.2% reduction in viral load following treatment (t=8.608,
118 P=0.0010) is comparable to the results reported for the CVL218 PARP inhibitor (35.2-99.7% inhibition) at comparable concentrations (15).

120 At concentrations higher than 30 μM, and treatment durations exceeding 48 h, stenoparib displayed marked cytotoxicity to Vero E6 cells **(Fig. 2A),** which limited our capacity to
122 comprehensively test the activity of the drug. We used a stenoparib response software predictor to pre-assess the susceptibility of human tumor cells based on the quantitative activity of 414
124 genes (22). When applied to human cell lines used with SARS-CoV-2 (23), the algorithm

predicted that LLC-MK2 cells would be less sensitive to stenoparib toxicity than Vero E6 cells.
126 The cell line Calu-3, originally isolated from the pleural effusion of a patient with lung adenocarcinoma (24), was predicted to be even more resistant than LLC-MK2. We verified this
128 prediction for Calu-3 cells using stenoparib concentrations up to 60 μM, and exposure for up to 120 h, with no elevation in cytotoxicity over baseline conditions (t=8.237, P=0.0144) **(Fig. 2B)**.

130 **Calu-3 lung epithelial cells as a platform for SARS-CoV-2.** Since Calu-3 cells were more resistant to the toxic effects of stenoparib than Vero E6 cells, we utilized Calu-3 cells to
132 test the effectiveness of higher doses than were previously achievable with Vero E6. The viral plaque assay comprehensively assesses inhibitors on the viral intracellular lifecycle, from virus
134 entry, to multiplication, and cell to cell spread. Plaques result from cell damage and death following infection, appearing as empty regions or "dead zones" in the cell monolayer (25).
136 Fresh media containing 2% FBS, with or without stenoparib or C/E control inhibitors, was applied to confluent monolayers of Calu-3 cells, which were then infected with SARS-CoV-2 for
138 1 h. At this time the infection media was removed, and the cells were overlaid with a semisolid matrix consisting of cell growth medium in 1.2% low melting temperature agarose, with or
140 without stenoparib or control inhibitors. At 120 h post infection, cells were fixed with paraformaldehyde, stained with crystal violet, and the number of plaques were visually counted.
142 As shown in **Fig. 3A** (see also **Fig. S1**), treatment with 30 μM stenoparib resulted in a 30.6% reduction of plaque forming units (PFUs) per well compared to infected, untreated cells (t=3.054,
144 P=0.0379). Using a higher dose of 60 μM stenoparib, we observed near complete inhibition of plaque formation (94.0%; t=10.24, P=0.0005) with no significant cytotoxicity (t=0.446,
146 P=0.6992), approaching the effect of the C/E control inhibitor (Fig. S1). These observations are mirrored by the results from RT-qPCR, which showed an 80.6% reduction of viral copy number

148 with 60 μM stenoparib (P<0.0001). These observations affirm the prediction that Calu-3 cells are more resistant to the effects of stenoparib than Vero E6 cells and are suitable hosts for SARS-
150 CoV-2 *in vitro*. It is interesting to speculate that Calu-3 cells may exhibit a degree of resistance to conditions that can be rapidly toxic in other, more rapidly dividing cell lines, which warrants
152 further exploration. Indeed, the *in vitro* doubling time of Calu-3 cells (>60 h) was notably slower than either the Vero E6 (~24 h) or the LLC-MK2 (~36 h) cell lines.

154 **The NL63 virus as a surrogate *in vitro* model.** In addition to SARS-CoV-2, several other human coronaviruses, including SARS-CoV, interact with human cells via the ACE2
156 receptor, and multiply intracellularly utilizing similar pathways (9). This group includes the respiratory coronavirus HCoV-NL63 (or just 'NL63'), which is a cause of the seasonal colds in
158 humans. While symptoms are generally mild, NL63 infections can be serious in infants and immunocompromised individuals (26-28). Based on its relatedness to SARS-CoV-2, and to
160 establish a surrogate system for use in Biosafety Level-2 (BSL-2) instead of BSL-3 laboratory conditions, we evaluated NL63 for testing the effects of stenoparib.

162 The NL63 virus (NR-470) was propagated in LLC-MK2 Rhesus macaque kidney cells (29). Viral replication levels were assessed by plaque assay and RT-qPCR as performed for
164 SARS-CoV-2. Controls were infected/untreated cells, and infected cells treated with the C/E inhibitor cocktail. Overall, the effects of stenoparib on NL63 corroborated the results of our
166 experiments with SARS-CoV-2. Treatment resulted in a dose-dependent decrease in virus replication, achieving a 69.3% and 95.8% reduction of plaquing efficiency and viral copy
168 number with 30 μM stenoparib, measured by plaque assay and RT-qPCR, respectively, compared to untreated controls (t=7.982 and 12.82, P=0.0002 for both) **(Fig. 4A and Fig. 4B)**.

170 **Identifying effects of stenoparib on the coronavirus lifecycle.** Coronavirus inhibitors may target one or several intracellular growth stages, including virus entry (camostat mesylate,
172 hydroxychloroquine), endosomal processing (hydroxychloroquine, rapamycin), translation and RNA processing (lopinavir), and transcription and replication (remdesivir) (1, 11, 30). By
174 altering the time of addition (TOA) and duration of treatment *in vitro*, we can discern whether a drug affects virus entry, intracellular growth, or both. TOA experiments were conducted using
176 the viral plaque assay with NL63 as a surrogate for SARS-CoV-2. RT-qPCR was performed in parallel to measure viral loads. We used remdesivir as a reference inhibitor, since its mechanism,
178 target and dosage range are known (31). Experiments to determine the lifecycle stages affected by stenoparib were performed as follows: **a)** to ascertain the effect on virus entry, cells were
180 transiently exposed to compounds starting 1 h before infection, and ending 1 h after infection; **b)** for effects on post-entry events, including transcription, processing, translation or replication,
182 compounds were added 1 h after infection, when a number of virions would have already entered cells, and treatment was continued until the experimental endpoint at 120 h; **c)** to examine the
184 maximum achievable effect of the compounds, a full-time assay was performed. Treatment was initiated simultaneously with virus infection and continued until the 120 h endpoint (see
186 **Methods** for a detailed description).

As shown in **Fig. 5A,** the antiviral activity of stenoparib is most notable when added
188 post-infection. The 60 μM stenoparib dose achieved complete inhibition of NL63 plaquing, with no detectable (N/D) plaques following post-entry treatment compared to untreated cells
190 ($P<0.0001$). This is on par with the effect of 4 μM remdesivir, which also eliminated plaque formation. Likewise, assay results for the full-time treatment were comparable between
192 stenoparib and remdesivir, with 88.4% reduction in plaque efficiency for stenoparib ($t=5.582$,

P=0.0051), and full inhibition for remdesivir vs. untreated cells. This is consistent with our
194 results from RT-qPCR, where stenoparib produced 98.7% (t=9.988, P=0.0099) and 95.5%
(t=9.663, P=0.0105) inhibition vs. untreated controls for post-entry and full-time drug exposure,
196 and also comparable to the activity of remdesivir. These data are in line with those reported
previously for the CVL218 PARP inhibitor and remdesivir (15).

198 With the plaque assay, we noticed a 16.5% reduction in plaque formation following
transient treatment with stenoparib early in the infection time course (i.e. 'Entry'; **Fig. 5A**). This
200 effect was not markedly different than the results recorded for remdesivir (-27.8%; t=1.919,
P=0.1275). Inhibition of virus entry is not expected for remdesivir since its activity is specific to
202 blocking of RNA replication (31, 32), which is a mid-late event in the viral lifecycle. In contrast,
our results from RT-qPCR strongly support a specific effect for stenoparib on inhibiting virus
204 entry, where a 37.9% reduction in viral load is observed in the entry assay compared to just a
3.1% reduction for remdesivir (t=4.352, P=0.0121) (**Fig. 5B**). Effects on viral entry are
206 consistent with the predicted activity of stenoparib on processes involved in early coronavirus
infection events (**see Discussion**). Taken as a whole, these observations suggest that stenoparib
208 may affect multiple targets that play roles in the early and late stages of coronavirus intracellular
multiplication.

210 **The combination of stenoparib and remdesivir strongly inhibits NL63.** Combination
drug therapies are widely used for the treatment for some of the worst human diseases, including
212 cancer (33), HIV/AIDS (34), and multidrug-resistant tuberculosis (35). The strategy of
combination therapy seeks to increase the beneficial effects of multiple drugs, lower their doses
214 to reduce adverse effects, and minimize the induction of resistance (36). Generally, the activity
of a drug combination is considered additive when the combined effect of two drugs is

216 equivalent to their individual doses, while if the effect is less than additive, the combination is considered antagonistic. Synergy occurs when the combined effect is greater than the additive
218 effect (36). Combinations of two or more drugs may lead to a synergistic effect by combining different mechanisms of action (MOA). Examples of synergistic combinations of drugs with
220 distinct MOAs include streptomycin–penicillin (37), trimethoprim–sulfa drugs (Co-trimoxazole) (38), and β-lactam/β-lactamase inhibitor combinations such as amoxicillin-clavulanate (39)
222 against bacterial infections.

Based on the fact that stenoparib and remdesivir inhibit coronavirus by distinct MOAs
224 (31, 32, 40), we approximated the half maximal effective concentration (EC_{50}) of stenoparib and remdesivir as 25.5 μM and 0.46 μM using the NL63 virus and plaque assays. Calculations were
226 aided by the online calculator from AAT Bioquest ("Quest Graph™ EC50 Calculator." *AAT Bioquest, Inc*, 26 Oct. 2020, https://www.aatbio.com/tools/ec50-calculator). We hypothesized
228 that a combination of stenoparib and remdesivir would be more potent than the individual compounds. To test this, we combined a range of doses of stenoparib with 0.5 μM remdesivir
230 and tested these for activity against NL63.

As shown in **Fig. 6**, complete inhibition of NL63 plaque formation was achieved with 60
232 μM stenoparib, in line with our earlier results with SARS-CoV-2 and Calu-3 cells **(Fig. 3).** Complete inhibition was also achieved with 1.0 μM remdesivir. However, a combination of 10
234 μM stenoparib and 0.5 μM remdesivir was more effective than either compound alone at these doses, achieving 90.7% inhibition for the combination, vs. 18.5% inhibition for 10 μM
236 stenoparib, and 65.6% for 0.5 μM remdesivir, suggesting at least additive effects when the drugs are combined. Notably, the stenoparib dose (10 μM) used in the combination is far below the

238 compound's EC_{50} of 25.5 μM. Altogether, these results support investigating the use of stenoparib and remdesivir as a combinatorial therapy for SARS-family coronavirus infections.

240

Discussion

242 Prior to the emergence of COVID-19, attempts to identify inhibitors of coronavirus were mainly focused on SARS- and MERS-CoVs. The recent efforts to develop COVID-19
244 therapeutics spans the gamut from new drug discovery to repurposing existing drugs. There are some excellent reviews on the subject (17, 41). Here, we focus on the compound stenoparib,
246 formerly known as 2X-121, an inhibitor of the cellular enzyme PARP-1/2. Stenoparib is thought to inhibit SARS-CoV-2 by multiple mechanisms, predominately by inhibiting of ADP-
248 ribosylation of proteins required for virus replication and assembly (42). ADP-ribosylation is a conserved, post-translational modification that is key for proper formation of the coronavirus
250 nucleocapsid, and inhibition can negatively affect packaging of the viral genome and virion stability. Specific targets of ADP-ribosylation include viral nsp3 protein, which is essential for
252 virulence and a component of the replication/transcription complex (RTC) (43, 44). Moreover, PARP inhibitors may exert additional protective effects at the host and cellular levels by
254 reducing depletion of NAD+ and ATP that leads to cell necrosis (40), as well as decreasing the pro-inflammatory NF-kB-triggered cytokine storm that can damage host organs (45). It has also
256 been suggested that PARP inhibitors enhance the degradation of the host type I interferon receptor (IFN-1R), which would also have a modulatory effect on the host inflammatory
258 response (46).

In this study, inhibition of SARS-family coronaviruses by stenoparib *in vitro* is likely due
260 to interference with multiple stages of the virus lifecycle. Consistent with its predicted mechanism, stenoparib is effective when introduced post-infection. Additionally, we noted an
262 association between stenoparib treatment and decreased virus counts soon after infection. This may reflect activity against multiple targets, including those involved in promoting virus entry.

264 Stenoparib interference with the activity of tankyrase and Wnt/β-catenin signaling can downregulate expression of the ACE2 receptor, leading to a decrease in the number of viruses
266 that can enter the cell, which is consistent with effects on virus entry and with our observations. In contrast, inhibition by remdesivir was predominately on post-entry events – its effect on virus
268 entry was minimal at best, which is in line with its specific MOA of targeting the virus replication machinery. Overall, our observations imply multiple mechanisms for stenoparib,
270 including impeding of viral entry and intracellular growth via modifications of multiple viral and host proteins.

272 Other human coronaviruses that utilize ACE2 for binding and entry may be suitable as surrogate platforms for the study of SARS-CoV-2 *in vitro,* so long as they can be propagated in
274 the laboratory and are able to elicit cellular infection phenotypes that can be quantitatively measured. We show that the human seasonal coronavirus NL63, which can cause a cold-like
276 illness in humans (26), is such an example. Like SARS-CoV-2 and SARS-CoV, NL63 is internalized following the binding of viral S-complex proteins to the ACE2 receptor (28, 47-49).
278 According to our observations, NL63 is susceptible to inhibition by compounds that affect SARS-CoV-2, including remdesivir, the protease inhibitors camostat mesylate and E64d, and
280 stenoparib, the subject of this study.

In light of the *in vitro* cytotoxic effects of stenoparib, we were unable to test it in Vero E6
282 cells against SARS-CoV-2 at doses exceeding 30 μM. Stenoparib was developed as a cytotoxic drug for cancer treatment (14), so it is not surprising that it showed dose-dependent cytotoxicity
284 against rapidly-dividing Vero E6 cells. PARP inhibitors typically express their lethality after several replication cycles (50). The susceptibility of Vero E6 cells to stenoparib toxicity may be
286 linked to its fast-growing phenotype, since two replication cycles can be achieved in as little as

48 h. Although LLC-MK2 cells, which are utilized for propagation and testing of NL63 are
288 substantially more resistant to stenoparib, their susceptibility to SARS-CoV-2 infection is
suboptimal. We were thus presented with a conundrum in how to test high doses of stenoparib
290 against SARS-CoV-2 to assess its maximum activity. This was addressed through the use of the
Calu-3 human lung carcinoma cell line to model SARS-CoV-2 infections. Our results confirm
292 the suitability of Calu-3 as a host for SARS-CoV-2 and its high degree of resistance to stenoparib
toxicity. This characteristic of Calu-3 cells was predicted *in silico* using a method previously
294 employed on clinical tumor biopsies (22), and experimentally validated in this study. Infection of
Calu-3 monolayers with SARS-CoV-2 formed large, clearly visible plaques, and in this regard,
296 the performance of Calu-3 surpassed Vero E6. A notable characteristic of Calu-3 is its slow
growth properties, which may coincide with a general degree of resistance to compounds that
298 target essential cellular pathways and are toxic to more rapidly dividing cells.

A promising drug to emerge from COVID therapeutic trials is the nucleoside analog
300 remdesivir, which shows activity against phylogenetically diverse viruses including Ebola,
Nipah, respiratory syncytial virus (RSV), and coronaviruses such as SARS- and MERS-CoV
302 (51), SARS-CoV-2 (31) and, as reported here, the seasonal human HCoV-NL63. Reviews on the
MOA of remdesivir have been published (17, 41, 51). After entering the cell, remdesivir is triple
304 phosphorylated to form remdesivir-triphosphate, and this structure is thought to inhibit RNA
polymerase, resulting in chain termination. While the precise molecular mechanism is not clear
306 (51), the EC_{50} of remdesivir has been reported to be 0.77 μM for SARS-CoV-2 (31), which is in
line with our measurement of 0.54 μM for SARS-CoV-2, and comparable to our experimentally-
308 determined EC_{50} of 0.46 μM against NL63.

While remdesivir inhibits the viral replicon, our data support multiple targets for
310 stenoparib. Moreover, stenoparib and remdesivir may be a potent combination at inhibiting
SARS-family coronaviruses inside cells. A mixture of 10 μM stenoparib and 0.5 μM remdesivir
312 was more successful at inhibiting the NL63 virus than either compound alone at these doses.
Considering their distinct mechanisms and high potency, a combination of remdesivir and
314 stenoparib is likely to produce a synergistic effect on additional SARS-family coronaviruses,
including SARS-CoV-2. Studies involving this combination in susceptible COVID-19 animal
316 models are in line for efficacy testing.

318

Materials and Methods

320 The antiviral activity of stenoparib *in vitro* was assessed against the novel coronavirus SARS-CoV-2 isolate USA-WA1/2020 (BEI Resources, NIAID, NIH: SARS-Related
322 Coronavirus 2, Isolate USA-WA1/2020, NR-52281) and human coronavirus strain HCoV_NL63 (BEI Resources, NIAID, NIH NR-470). We used Vero E6 (ATCC CRL-1586) and Calu-3 cells
324 (ATCC HTB-55) from the American Type Culture Collection (ATCC, Manassas, VA, USA) in EMEM (Eagle's Minimum Essential Medium) supplemented with 2% or 10% fetal bovine serum
326 (FBS), 100 U/mL penicillin, 100 µg/mL streptomycin 'pen-strep', 0.01 M HEPES, 1 mM sodium pyruvate, 1x non-essential amino acids solution (SH3023801, Thermo Fisher), and 2 mM
328 L-glutamine, for the propagation and experimentation with SARS-CoV-2. LLC-MK2 cells (ATCC CCL-7), maintained in Medium 199 (M4530, Millipore Sigma) supplemented with FBS
330 and pen-strep, were used for the experiments with the NL63 coronavirus. Inhibition of viral replication was assessed using reverse-transcription quantitative real-time PCR (RT-qPCR) to
332 measure the number of virions released into the cellular supernatant.

Plaque assays. 6-well plates (CLS3516, Millipore Sigma) were seeded with ~3.0x10^5
334 cells/well and incubated for 48-72 h at 37°C in 5% CO_2 until 80-90% confluency was reached. Calu-3 cells were incubated for >10 days to achieve 80-90% confluency. Prior to infection the
336 media was replaced with fresh media containing 2.0% FBS with varying concentrations of stenoparib as appropriate for each experiment (see results) and infected with coronavirus (SARS-
338 CoV-2 or NL63) at an MOI of 0.013 for SARs-CoV-2 and 0.003 for NL63. Media was then replaced with a 1 X Dulbecco's MEM (DMEM - Millipore Sigma) / 1.2% low-melting agarose
340 (Bio-Rad) overlay containing the appropriate drug concentration for each experiment. This was allowed to solidify at room temperature for 15 minutes, and incubated for 120 h at 37°C in a 5%

342 CO2 atmosphere. A cocktail of the protease inhibitors camostat mesylate and E64d (C/E) was a control for all experiments (21). SARS-CoV-2 manipulations were conducted in a BSL-3
344 facility. 2.0 ml of 4% paraformaldehyde was added to each overlay for 30 minutes, followed by staining with 1.0% crystal violet, removal of the overlay, and a triple rinse with PBS. Plaque
346 forming units (pfu) were counted, averaged, and normalized to the untreated control group. Each run contained three biological replicates and was conducted a minimum of two times. Standard
348 deviation was calculated using the variation of averaged counts among all runs. Values were plotted using GraphPad Prism version 8.0.0 for Windows (GraphPad Software) and annotated
350 using Adobe Illustrator (Adobe Systems Incorporated). Statistical significance was determined using a parametric unpaired t-test in GraphPad Prism version 8.0.0.

352 **RT-qPCR: Infection and viral RNA extraction**. 12-well plates (CLS3513, Millipore Sigma) were seeded with ~1.0x10^5 cells/well and incubated until 80-90% confluency was
354 reached. Growth media was replaced and infected with coronavirus (SARS-CoV-2 or NL63) at an MOI of 0.04 for SARs-CoV-2 and 0.01 for NL63 for up to 120 h at 37°C in 5% CO2
356 atmosphere. C/E was used as a control inhibitor for all experiments. Each run contained two biological replicates and was conducted three times. 400 µL of supernatant was harvested at 48 h
358 for SARS-CoV-2, 120 h for NL63. RNA was extracted using Invitrogen Pure-Link RNA kits (Thermo Fisher) according to their recommendations.

360 **RT-qPCR: Signature identification and qPCR assay design.** Two TaqMan qPCR assays were designed for the SARS-CoV-2 or the NL63 coronaviruses. For NL63, the reference
362 genome (NC_005831) was divided into 200 nucleotide fragments, which were aligned against a set of 2,771 coronavirus genomes with BLAT v36.2 (52) in conjunction with LS-BSR v1.2.2
364 (53). Regions were identified that had a BLAST score ratio (BSR) (54) value ≥0.8 in 60 NL63

genomes, and a BSR value <0.4 in all other coronavirus genomes. A total of 10 fragments were
366 highly specific to all NL63 genomes. Primers and probes were identified using Primer3 v2.3.6
(55). A similar process was conducted for SARS-CoV-2 assay design, except the
368 GCF_009858895.2 reference genome was used. A total of 4 fragments were unique to 64 distinct
SARS-CoV-2 genomes. A probe was designed targeting the spike (S) protein furin cleavage site
370 with Primer3.

The SARS-CoV-2 qPCR amplified a 125 bp region of the S protein using forward primer
372 CoV2-S_19F (5'-GCTGAACATGTCAACAACTC-3') and reverse primer CoV2-S_143R (5'-
GCAATGATGGATTGACTAGC-3') with MGB TaqMan probe CoV2-S_93FP (5'-
374 ACTAATTCTCCTCGGCGGGC-3') labeled with FAM dye, which was designed based off the
SARS-CoV-2 genome GCF_009858895.2 (GenBank: MN908947.3), while the NL63 qPCR
376 amplified a 191 bp region of a membrane protein (GenBank: YP_003770.1) using forward
primer NL63_10F (5'-TGGTCGCTCTGTTAATGAAA-3') and reverse primer NL63_200R (5'-
378 AAATTTCTTCCTAGCAGCTC-3') with MGB TaqMan probe NL63_102RP (5'-
CCCTCCTGAGAGGCAACACC-3'), labeled with a VIC dye, which was based off the
380 HCoV_NL63 genome (GenBank: MN306040.1).

RT-qPCR: Reverse transcription and PCR amplification. We initially used a two-step
382 method where viral RNA was converted into cDNA using Invitrogen SuperScript IV VILO
Master Mix (11766500, Thermo Fisher) in 96-well format (18021-014, Thermo Fisher); in a
384 SimpliAmp® thermocycler (Applied Biosystems). 1 µL of template cDNA was then subjected to
qPCR in 10 µL reactions containing 1x TaqMan Universal Master Mix II (w/o AmpERASE
386 UNG), with 0.2 µM of each forward and reverse primer and 0.1 µM of probe for the SARS-
CoV-2 qPCR and 0.25 µM of each forward and reverse primer and 0.125 µM of probe for the

388 NL63 qPCR). Amplification was performed in triplicate using either a QuantStudio 7 flex or
QuantStudio 12K (Applied Biosystems) utilizing: 10' at 95°C, then 40 X at 95°C 15", 60°C for
390 1'. Another approach employed a one-step procedure in which viral RNA was converted to
cDNA using the TaqMan primers, followed by qPCR (4x Reliance One-Step Multiplex RT-
392 qPCR Supermix) with the same primers, probes, and concentrations as for the two-step approach.
Triplicate reactions were performed using QuantStudio under the following conditions: 50°C for
394 10'; 95°C, 10'; 40 cycles of 95°C 10" and 60°C 30". Positive amplification and non-template
controls were included on every run.

396 **RT-qPCR: Data analysis.** Synthetic double-stranded DNA fragments were generated
(gBlocks Gene Fragments, Integrated DNA Technologies) as qPCR controls, and contained
398 amplification primers for either SARS-CoV-2 or NL63 targets, and were elongated to 200 bp.
These gBlocks were resuspended according to the manufacturer's protocol and quantified using a
400 Qubit 4 fluorometer with a dsDNA HS assay kit (Q32851 Thermo Fisher), then normalized to
10^8 copies per µL. Using serial dilution, we were able to extrapolate viral copy number in each
402 of the experimental samples. Based on these standards, the QuantStudio instrument software
generated a curve to quantify sample reactions. The calculated quantities for each sample were
404 averaged, and the standard deviation was calculated among reactions. Values for the
experimental replicates and the standard deviations among experimental runs were averaged, and
406 then normalized to the untreated control group to obtain percent inhibition values. These were
plotted using GraphPad Prism version 8.0.0 for Windows and annotations were added using
408 Adobe Illustrator. Where appropriate, statistical significance was determined using a parametric
unpaired t-test in GraphPad Prism version 8.0.0.

410 **Cytotoxicity.** Cytotoxicity was measured using the Promega™ CytoTox 96™ Nonradioactive Cytotoxicity Assay kit (G1780) in 50 μL reactions according to the
412 manufacturer's protocol. The absorbance at 490 nm (A490) was measured using a BioTeK Synergy™ HT plate reader model # 7091000. Relative cytotoxicity was calculated by dividing
414 the experimental LDH release as measured at 490nm by the maximum LDH release control multiplied by 100.

416 **Time of addition experiments.** For the full-time experiments, virus, drug and cells were incubated for 1 h. Media was then replaced with fresh media containing the drug. Entry
418 experiments were pretreated with drug for 1 h and then infected with virus for an additional hour, followed by media replacement that lacked drug. Post-entry experiments utilized cells that were
420 infected with virus for 1 h, and media was replaced with fresh media containing the drug. Statistical significance was determined using a parametric unpaired t-test in GraphPad Prism
422 version 8.0.0.

Stenoparib in combination with remdesivir. We performed plaque assays, and used
424 these data to estimate the EC_{50} of stenoparib and remdesivir (329511, MedKoo Biosciences, Morrisville, NC, USA) against NL63 (both drugs) and SARS-CoV-2 (remdesivir only) in LLC-
426 MK2 and Vero E6 cells according to results from at least two experimental runs. The EC_{50} values were approximated with the aid of the online calculator from AAT Bioquest ("Quest
428 Graph™ EC50 Calculator." *AAT Bioquest, Inc*, 26 Oct. 2020, https://www.aatbio.com/tools/ec50-calculator).

430

Acknowledgments

This research was supported by a grant from The Flinn Foundation and continuing support of The Cowden Endowment for Microbiology. Core experiments were supported by service fees paid by Allarity Therapeutics.

Conflict of Interest Statement

SK is employed by and holds a financial interest in Allarity Therapeutics, which stands to potentially benefit from these results.

References

1. Hu B, Guo H, Zhou P, Shi ZL. 2020. Characteristics of SARS-CoV-2 and COVID-19. Nature Reviews Microbiology doi:10.1038/s41579-020-00459-7.
2. Wu ZY, McGoogan JM. 2020. Characteristics of and Important Lessons From the Coronavirus Disease 2019 (COVID-19) Outbreak in China Summary of a Report of 72 314 Cases From the Chinese Center for Disease Control and Prevention. Jama-Journal of the American Medical Association 323:1239-1242.
3. Liu Y, Mao B, Liang S, Yang JW, Lu HW, Chai YH, Wang L, Zhang L, Li QH, Zhao L, He Y, Gu XL, Ji XB, Li L, Jie ZJ, Li Q, Li XY, Lu HZ, Zhang WH, Song YL, Qu JM, Xu JF, Treatment SC. 2020. Association between age and clinical characteristics and outcomes of COVID-19. European Respiratory Journal 55.
4. Wu C, Chen X, Cai Y. 2020. Risk factors associated with acute respiratory distress syndrome and death in patients with coronavirus disease 2019 pneumonia in Wuhan, China (vol 180, pg 934, 2020). Jama Internal Medicine 180:1031-1031.
5. Guan W, Ni Z, Hu Y, Liang W, Ou C, He J, Liu L, Shan H, Lei C, Hui DSC, Du B, Li L, Zeng G, Yuen KY, Chen R, Tang C, Wang T, Chen P, Xiang J, Li S, Wang JL, Liang Z, Peng Y, Wei L, Liu Y, Hu YH, Peng P, Wang JM, Liu J, Chen Z, Li G, Zheng Z, Qiu S, Luo J, Ye C, Zhu S, Zhong N, Grp CMTE. 2020. Clinical Characteristics of Coronavirus Disease 2019 in China. New England Journal of Medicine 382:1708-1720.
6. Dong E, Du H, Gardner L. 2020. An interactive web-based dashboard to track COVID-19 in real time. Lancet Infect Dis 20:533-534.
7. Impact JHCfC. 2020. Coronavirus Resource Center - COVID Tracker. https://www.arcgis.com/apps/opsdashboard/index.html#/409af567637846e3b5d4182fcd779bea. Accessed
8. Team IC-F. 2020. Modeling COVID-19 scenarios for the United States. Nat Med doi:10.1038/s41591-020-1132-9.
9. Rabi FA, Al Zoubi MS, Kasasbeh GA, Salameh DM, Al-Nasser AD. 2020. SARS-CoV-2 and Coronavirus Disease 2019: What We Know So Far. Pathogens 9.
10. Hoffmann M, Kleine-Weber H, Schroeder S, Kruger N, Herrler T, Erichsen S, Schiergens TS, Herrler G, Wu NH, Nitsche A, Muller MA, Drosten C, Pohlmann S. 2020. SARS-CoV-2 Cell Entry Depends on ACE2 and TMPRSS2 and Is Blocked by a Clinically Proven Protease Inhibitor. Cell 181:271-280 e8.
11. Poduri R, Joshi G, Jagadeesh G. 2020. Drugs targeting various stages of the SARS-CoV-2 life cycle: Exploring promising drugs for the treatment of Covid-19. Cell Signal 74:109721.
12. Astuti I, Ysrafil. 2020. Severe Acute Respiratory Syndrome Coronavirus 2 (SARS-CoV-2): An overview of viral structure and host response. Diabetes Metab Syndr 14:407-412.
13. Dziadkowiec KN, Gasiorowska E, Nowak-Markwitz E, Jankowska A. 2016. PARP inhibitors: review of mechanisms of action and BRCA1/2 mutation targeting. Prz Menopauzalny 15:215-219.
14. McGonigle S, Chen ZH, Wu JY, Chang P, Kolber-Simonds D, Ackermann K, Twine NC, Shie JL, Miu JZT, Huang KC, Moniz GA, Nomoto K. 2015. E7449: A dual inhibitor of PARP1/2 and tankyrase1/2 inhibits growth of DNA repair deficient tumors and antagonizes Wnt signaling. Oncotarget 6:41307-41323.
15. Ge Y, Tian T, Huang S, Wan F, Li J, Li S, Yang H, Hong L, Wu N, Yuan E, Cheng L, Lei Y, Shu H, Feng X, Jiang Z, Chi Y, Guo X, Cui L, Xiao L, Li Z, Yang C, Miao Z, Tang H, Chen L, Zeng H, Zhao D, Zhu F, Shen X, Zeng J. 2020. A data-driven drug repositioning

framework discovered a potential therapeutic agent targeting COVID-19. bioRxiv doi:10.1101/2020.03.11.986836:2020.03.11.986836.

16. Pushpakom S, Iorio F, Eyers PA, Escott KJ, Hopper S, Wells A, Doig A, Guilliams T, Latimer J, McNamee C, Norris A, Sanseau P, Cavalla D, Pirmohamed M. 2018. Drug repurposing: progress, challenges and recommendations. Nat Rev Drug Discov doi:10.1038/nrd.2018.168.

17. Saha RP, Sharma AR, Singh MK, Samanta S, Bhakta S, Mandal S, Bhattacharya M, Lee SS, Chakraborty C. 2020. Repurposing Drugs, Ongoing Vaccine, and New Therapeutic Development Initiatives Against COVID-19. Front Pharmacol 11:1258.

18. Zhou YD, Hou Y, Shen JY, Huang Y, Martin W, Cheng FX. 2020. Network-based drug repurposing for novel coronavirus 2019-nCoV/SARS-CoV-2. Cell Discovery 6.

19. Qinfen Z, Jinming C, Xiaojun H, Huanying Z, Jicheng H, Ling F, Kunpeng L, Jingqiang Z. 2004. The life cycle of SARS coronavirus in Vero E6 cells. J Med Virol 73:332-7.

20. Ogando NS, Dalebout TJ, Zevenhoven-Dobbe JC, Limpens R, van der Meer Y, Caly L, Druce J, de Vries JJC, Kikkert M, Barcena M, Sidorov I, Snijder EJ. 2020. SARS-coronavirus-2 replication in Vero E6 cells: replication kinetics, rapid adaptation and cytopathology. J Gen Virol 101:925-940.

21. Li J, Zhan P, Liu X. 2020. Targeting the entry step of SARS-CoV-2: a promising therapeutic approach. Signal Transduct Target Ther 5:98.

22. Plummer R, Dua D, Cresti N, Drew Y, Stephens P, Foegh M, Knudsen S, Sachdev P, Mistry BM, Dixit V, McGonigle S, Hall N, Matijevic M, McGrath S, Sarker D. 2020. First-in-human study of the PARP/tankyrase inhibitor E7449 in patients with advanced solid tumours and evaluation of a novel drug-response predictor. Br J Cancer 123:525-533.

23. Chu H, Chan JF, Yuen TT, Shuai H, Yuan S, Wang Y, Hu B, Yip CC, Tsang JO, Huang X, Chai Y, Yang D, Hou Y, Chik KK, Zhang X, Fung AY, Tsoi HW, Cai JP, Chan WM, Ip JD, Chu AW, Zhou J, Lung DC, Kok KH, To KK, Tsang OT, Chan KH, Yuen KY. 2020. Comparative tropism, replication kinetics, and cell damage profiling of SARS-CoV-2 and SARS-CoV with implications for clinical manifestations, transmissibility, and laboratory studies of COVID-19: an observational study. Lancet Microbe 1:e14-e23.

24. Fogh J, Fogh JM, Orfeo T. 1977. One hundred and twenty-seven cultured human tumor cell lines producing tumors in nude mice. J Natl Cancer Inst 59:221-6.

25. Baer A, Kehn-Hall K. 2014. Viral concentration determination through plaque assays: using traditional and novel overlay systems. J Vis Exp doi:10.3791/52065:e52065.

26. van der Hoek L, Pyrc K, Berkhout B. 2006. Human coronavirus NL63, a new respiratory virus. FEMS Microbiol Rev 30:760-73.

27. Glowacka I, Bertram S, Herzog P, Pfefferle S, Steffen I, Muench MO, Simmons G, Hofmann H, Kuri T, Weber F, Eichler J, Drosten C, Pohlmann S. 2010. Differential downregulation of ACE2 by the spike proteins of severe acute respiratory syndrome coronavirus and human coronavirus NL63. J Virol 84:1198-205.

28. Li W, Sui J, Huang IC, Kuhn JH, Radoshitzky SR, Marasco WA, Choe H, Farzan M. 2007. The S proteins of human coronavirus NL63 and severe acute respiratory syndrome coronavirus bind overlapping regions of ACE2. Virology 367:367-74.

29. Schildgen O, Jebbink MF, de Vries M, Pyrc K, Dijkman R, Simon A, Muller A, Kupfer B, van der Hoek L. 2006. Identification of cell lines permissive for human coronavirus NL63. J Virol Methods 138:207-10.

30. Omarjee L, Janin A, Perrot F, Laviolle B, Meilhac O, Mahe G. 2020. Targeting T-cell senescence and cytokine storm with rapamycin to prevent severe progression in COVID-19. Clin Immunol 216:108464.

31. Wang M, Cao R, Zhang L, Yang X, Liu J, Xu M, Shi Z, Hu Z, Zhong W, Xiao G. 2020. Remdesivir and chloroquine effectively inhibit the recently emerged novel coronavirus (2019-nCoV) in vitro. Cell Res 30:269-271.

32. Chang CK, Jeyachandran S, Hu NJ, Liu CL, Lin SY, Wang YS, Chang YM, Hou MH. 2016. Structure-based virtual screening and experimental validation of the discovery of inhibitors targeted towards the human coronavirus nucleocapsid protein. Mol Biosyst 12:59-66.
33. Bigioni M, Benzo A, Irrissuto C, Lopez G, Curatella B, Maggi CA, Manzini S, Crea A, Caroli S, Cubadda F, Binaschi M. 2008. Antitumour effect of combination treatment with Sabarubicin (MEN 10755) and cis-platin (DDP) in human lung tumour xenograft. Cancer Chemother Pharmacol 62:621-9.
34. Casado JL, Banon S. 2015. Dutrebis (lamivudine and raltegravir) for use in combination with other antiretroviral products for the treatment of HIV-1 infection. Expert Rev Clin Pharmacol 8:709-18.
35. Caminero JA, Sotgiu G, Zumla A, Migliori GB. 2010. Best drug treatment for multidrug-resistant and extensively drug-resistant tuberculosis. Lancet Infect Dis 10:621-9.
36. Garcia-Fuente A, Vazquez F, Vieitez JM, Garcia Alonso FJ, Martin JI, Ferrer J. 2018. CISNE: An accurate description of dose-effect and synergism in combination therapies. Sci Rep 8:4964.
37. Reynolds B, Rowley D. 1953. Synergism between streptomycin and penicillin. British journal of experimental pathology 34:651-655.
38. Nichols RJ, Sen S, Choo YJ, Beltrao P, Zietek M, Chaba R, Lee S, Kazmierczak KM, Lee KJ, Wong A, Shales M, Lovett S, Winkler ME, Krogan NJ, Typas A, Gross CA. 2011. Phenotypic landscape of a bacterial cell. Cell 144:143-56.
39. Yogev R, Melick C, Kabat WJ. 1981. In vitro and in vivo synergism between amoxicillin and clavulanic acid against ampicillin-resistant Haemophilus influenzae type b. Antimicrobial agents and chemotherapy 19:993-996.
40. Kouhpayeh S, Shariati L, Boshtam M, Rahimmanesh I, Mirian M, Zeinalian M, Salari-jazi A, Khanahmad N, Damavandi MS, Sadeghi P, Khanahmad H. 2020. The molecular story of COVID-19; NAD+ depletion addresses all questions in this infection. preprint preprint doi:10.20944/preprints202003.0346.v1.
41. Pillaiyar T, Meenakshisundaram S, Manickam M. 2020. Recent discovery and development of inhibitors targeting coronaviruses. Drug Discov Today 25:668-688.
42. Grunewald ME, Fehr AR, Athmer J, Perlman S. 2018. The coronavirus nucleocapsid protein is ADP-ribosylated. Virology 517:62-68.
43. Lei J, Kusov Y, Hilgenfeld R. 2018. Nsp3 of coronaviruses: Structures and functions of a large multi-domain protein. Antiviral Res 149:58-74.
44. Fehr AR, Athmer J, Channappanavar R, Phillips JM, Meyerholz DK, Perlman S. 2015. The nsp3 macrodomain promotes virulence in mice with coronavirus-induced encephalitis. J Virol 89:1523-36.
45. Gharote MA. 2020. Role of poly (ADP) ribose polymerase-1 inhibition by nicotinamide as a possible additive treatment to modulate host immune response and prevention of cytokine storm in COVID-19. Indian Journal of Medical Sciences 72:25-28.
46. Coperchini F, Chiovato L, Croce L, Magri F, Rotondi M. 2020. The cytokine storm in COVID-19: An overview of the involvement of the chemokine/chemokine-receptor system. Cytokine Growth Factor Rev 53:25-32.
47. Smith MK, Tusell S, Travanty EA, Berkhout B, van der Hoek L, Holmes KV. 2006. Human angiotensin-converting enzyme 2 (ACE2) is a receptor for human respiratory coronavirus NL63. Adv Exp Med Biol 581:285-8.
48. Pohlmann S, Gramberg T, Wegele A, Pyrc K, van der Hoek L, Berkhout B, Hofmann H. 2006. Interaction between the spike protein of human coronavirus NL63 and its cellular receptor ACE2. Adv Exp Med Biol 581:281-4.
49. Lin HX, Feng Y, Wong G, Wang L, Li B, Zhao X, Li Y, Smaill F, Zhang C. 2008. Identification of residues in the receptor-binding domain (RBD) of the spike protein of

human coronavirus NL63 that are critical for the RBD-ACE2 receptor interaction. J Gen Virol 89:1015-1024.
50. Garnett MJ, Edelman EJ, Heidorn SJ, Greenman CD, Dastur A, Lau KW, Greninger P, Thompson IR, Luo X, Soares J, Liu Q, Iorio F, Surdez D, Chen L, Milano RJ, Bignell GR, Tam AT, Davies H, Stevenson JA, Barthorpe S, Lutz SR, Kogera F, Lawrence K, McLaren-Douglas A, Mitropoulos X, Mironenko T, Thi H, Richardson L, Zhou W, Jewitt F, Zhang T, O'Brien P, Boisvert JL, Price S, Hur W, Yang W, Deng X, Butler A, Choi HG, Chang JW, Baselga J, Stamenkovic I, Engelman JA, Sharma SV, Delattre O, Saez-Rodriguez J, Gray NS, Settleman J, Futreal PA, Haber DA, et al. 2012. Systematic identification of genomic markers of drug sensitivity in cancer cells. Nature 483:570-5.
51. Saha A, Sharma AR, Bhattacharya M, Sharma G, Lee SS, Chakraborty C. 2020. Probable Molecular Mechanism of Remdesivir for the Treatment of COVID-19: Need to Know More. Arch Med Res 51:585-586.
52. Kent WJ. 2002. BLAT--the BLAST-like alignment tool. Genome Res 12:656-64.
53. Sahl JW, Caporaso JG, Rasko DA, Keim P. 2014. The large-scale blast score ratio (LS-BSR) pipeline: a method to rapidly compare genetic content between bacterial genomes. PeerJ 2:e332.
54. Rasko DA, Myers GS, Ravel J. 2005. Visualization of comparative genomic analyses by BLAST score ratio. BMC Bioinformatics 6:2.
55. Rozen S, Skaletsky H. 2000. Primer3 on the WWW for general users and for biologist programmers. Methods Mol Biol 132:365-86.

Figures

616 **Fig. 1. Stenoparib exhibits dose-dependent inhibition of SARS-CoV-2 as measured by RT-qPCR.** RT-qPCR was performed on viral RNA collected from cell culture supernatants at 48 h
618 post infection. Replicates within each run were averaged, and a total of three experiments were performed. Error bars were based on averaged standard deviations within runs. Cytotoxicity
620 against Vero E6 cells was determined at 48 h using the Promega™ CytoTox 96™ assay kit, and values represent the average of the two independent experiments (reported in Fig. 2A).

622

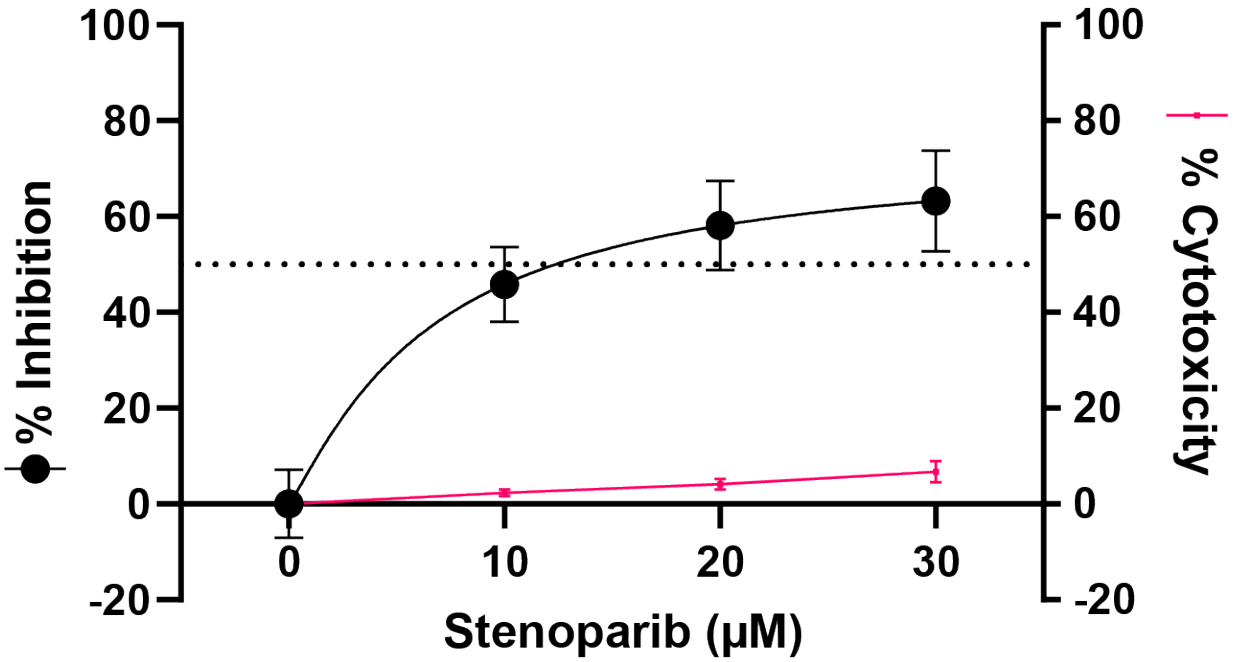

624

626 **Fig. 2. Stenoparib is cytotoxic in Vero E6 cells at concentrations greater than 30 µM, but not in Calu-3 cells.** Cytotoxicity was determined using the Promega™ CytoTox 96™ lactate-
628 dehydrogenase-release assay kit by harvesting culture media every 24 h up to 120 h post exposure. **A)** Vero E6 cells; **B)** Calu-3 cells, with 10, 20, 30, and 60 µM of stenoparib.
630 Measurements were normalized to cells treated with 1.0% Triton X-100 and compared to untreated controls. Biological replicates from two runs were averaged, and median values are
632 plotted. Results are representative of two experiments, and error bars are based on the standard deviation.

634

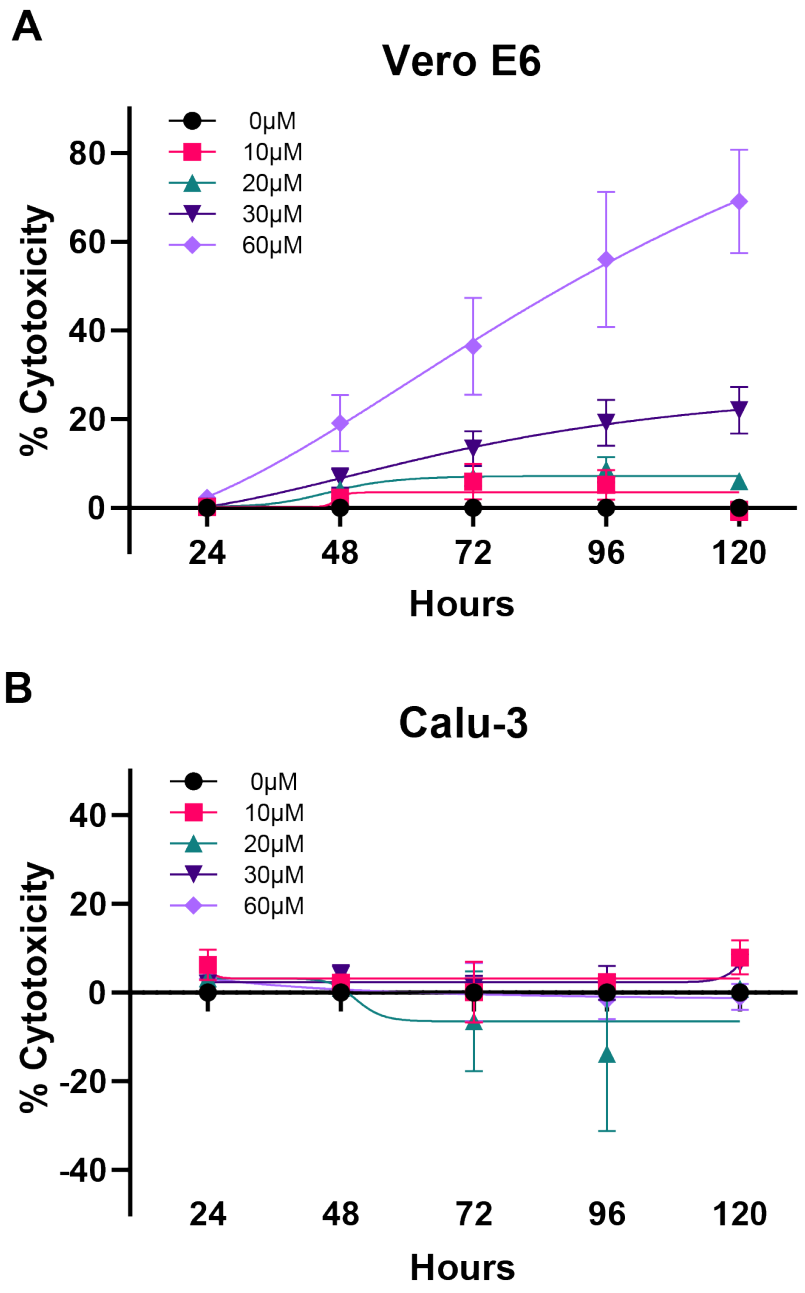

636 **Fig. 3. Stenoparib exhibits dose-dependent inhibition of SARS-CoV-2 in Calu-3 cells. A)**
Plaque forming efficiency using SARS-CoV-2. Values are normalized as a percentage of
638 inhibition compared to infected, but untreated cells. Plaques were counted 120 h after infection,
replicates from each run were averaged, and assays were performed three times. Error bars are
640 based on the standard deviation across all runs. **B)** RT-qPCR was performed on viral RNA
collected from cell culture supernatants at 48 h post infection and replicate values within each
642 run were averaged; a total of three runs were performed. Error bars are based on averaged
standard deviations within runs. Cytotoxicity against Calu-3 cells was determined at 48 and 120
644 h, as appropriate, using the Promega™ CytoTox 96™ assay kit, and values represent the average
of the two independent experiments (reported in Fig. 2B).

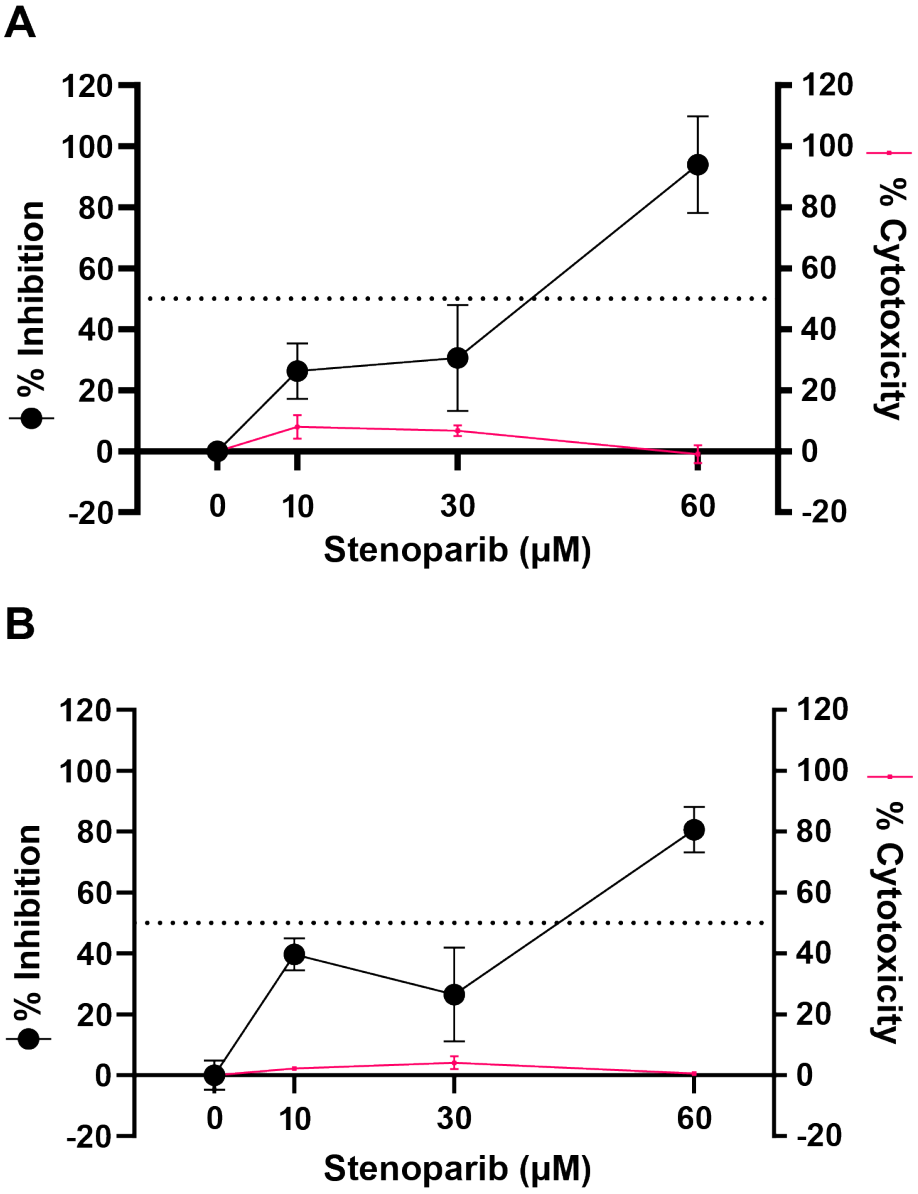

646

648

Fig. 4. Stenoparib exhibits dose-dependent inhibition of HCoV-NL63 in LLC-MK2 cells. A) Plaquing efficiency values are normalized as a percentage of inhibition compared to infected, but untreated cells. Plaques were counted 120 h after infection, and assays were performed three times. Error bars are based on the standard deviation across all runs. **B)** RT-qPCR was performed on viral RNA collected from cell culture media at 120 h post infection. Biological replicates from each run were averaged, and three independent runs were performed. Error bars were based on averaged standard deviations within runs. Cytotoxicity against LLC-MK2 cells was determined at 120 h using the Promega™ CytoTox 96™ assay kit, and values represent the average of the three independent experiments.

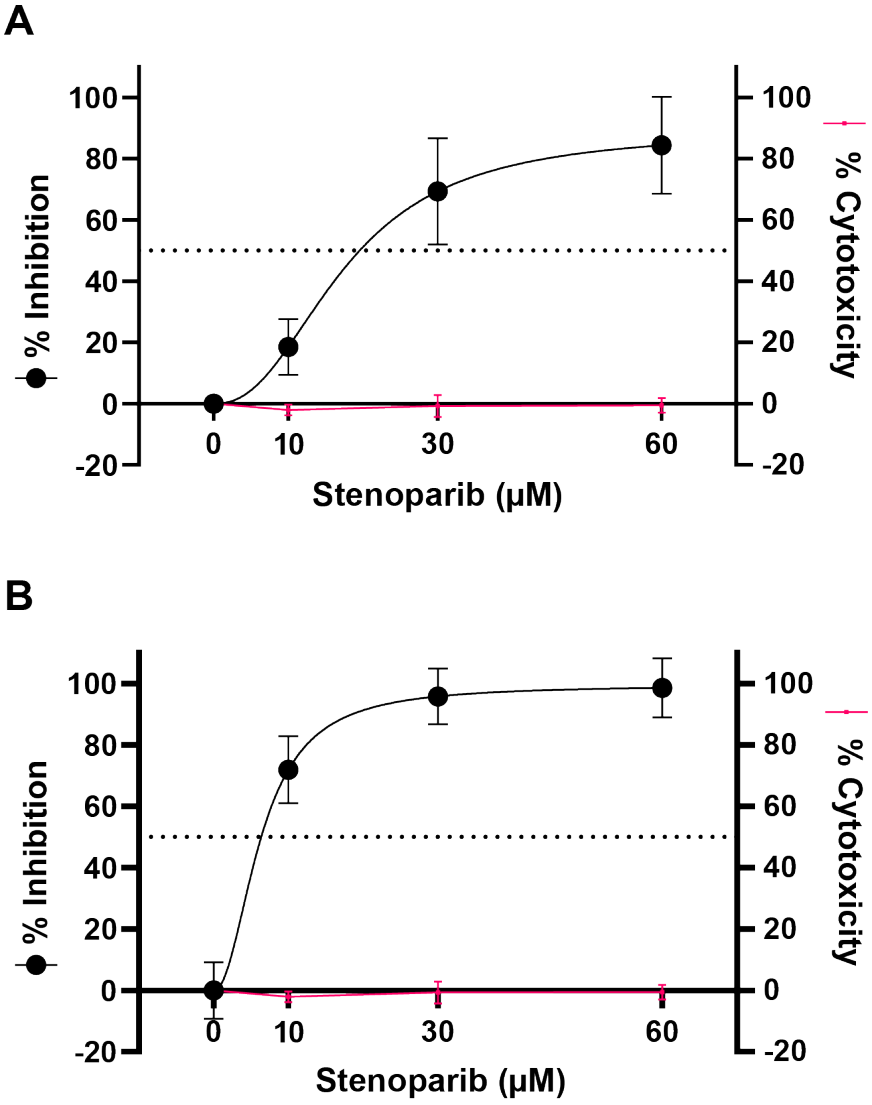

Fig. 5. Stenoparib inhibits HCoV-NL63 entry and post entry events while remdesivir inhibits post-entry. A) Plaque assays were performed three times and replicate plaque forming unit counts from each run were averaged. Error bars are based on standard deviation among runs. Brackets indicate the t-test comparison and P-value for the "Entry" group. No significant difference was observed between stenoparib and remdesivir under any treatment. N/D indicates that no plaques were detected in these treatment groups. **B)** RT-qPCR was performed on viral RNA collected from cell culture media at 120 h post infection and replicate values within each run were averaged; a total of three runs were performed. Error bars were based on averaged standard deviations within runs. Brackets indicate the t-test comparison and P-value for the "Entry" group. Significant differences were observed between stenoparib and remdesivir under all treatments.

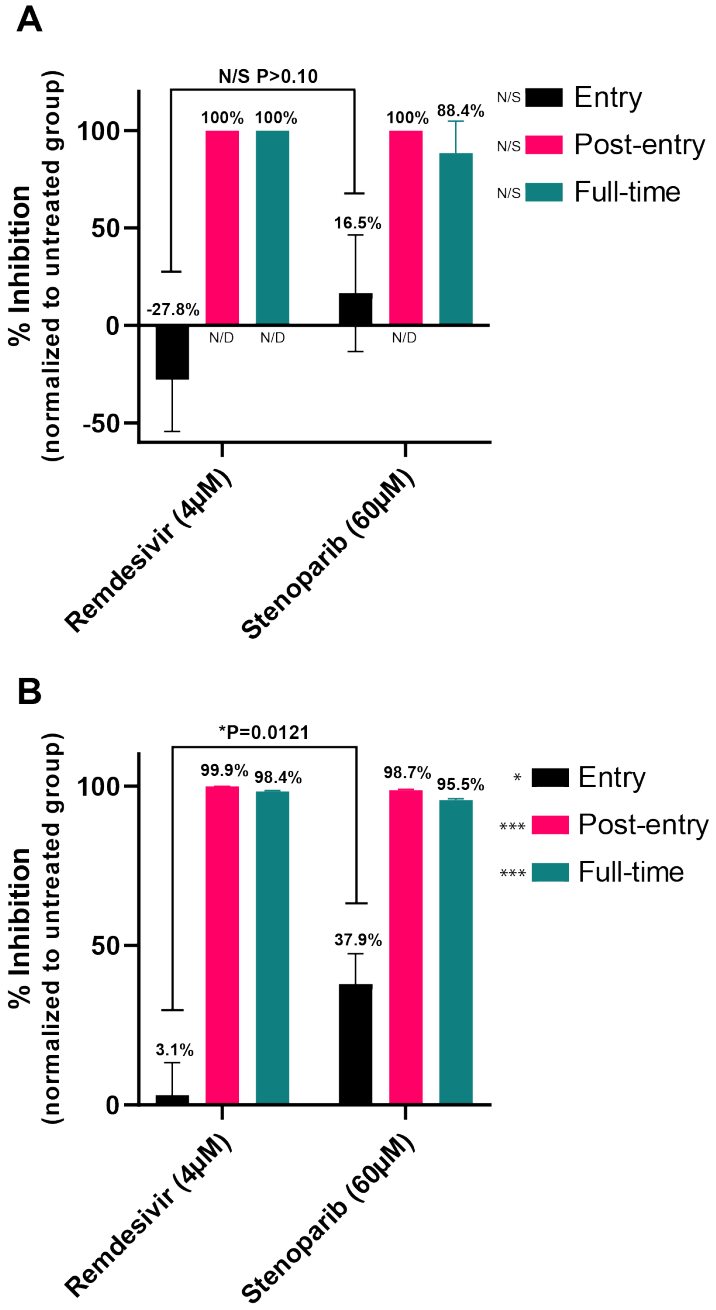

Fig. 6. Stenoparib and remdesivir in combination is a potent inhibitor of NL63. Plaque assays were performed a minimum of two times and replicate values from each run were averaged. Plaquing efficiency values are normalized as a percentage of inhibition compared to infected, but untreated cells. Three data sets are plotted to illustrate the treatment of NL63 with 1) stenoparib and 2) remdesivir as monotherapies and as a 3) combination therapy, whereby increasing concentrations of stenoparib are combined with 0.5 µM remdesivir; the EC_{50} was computationally approximated at 0.46 µM. The stenoparib monotherapy data is the same as previously reported (Fig. 4A). The synergistic activity threshold is defined as the sum of the mean values of 10 µM stenoparib and 0.5 µM remdesivir as monotherapies, while the grey highlighted area represents the minimum and maximum possible additive activity values based on the range of error for those same concentrations observed during these experiments.

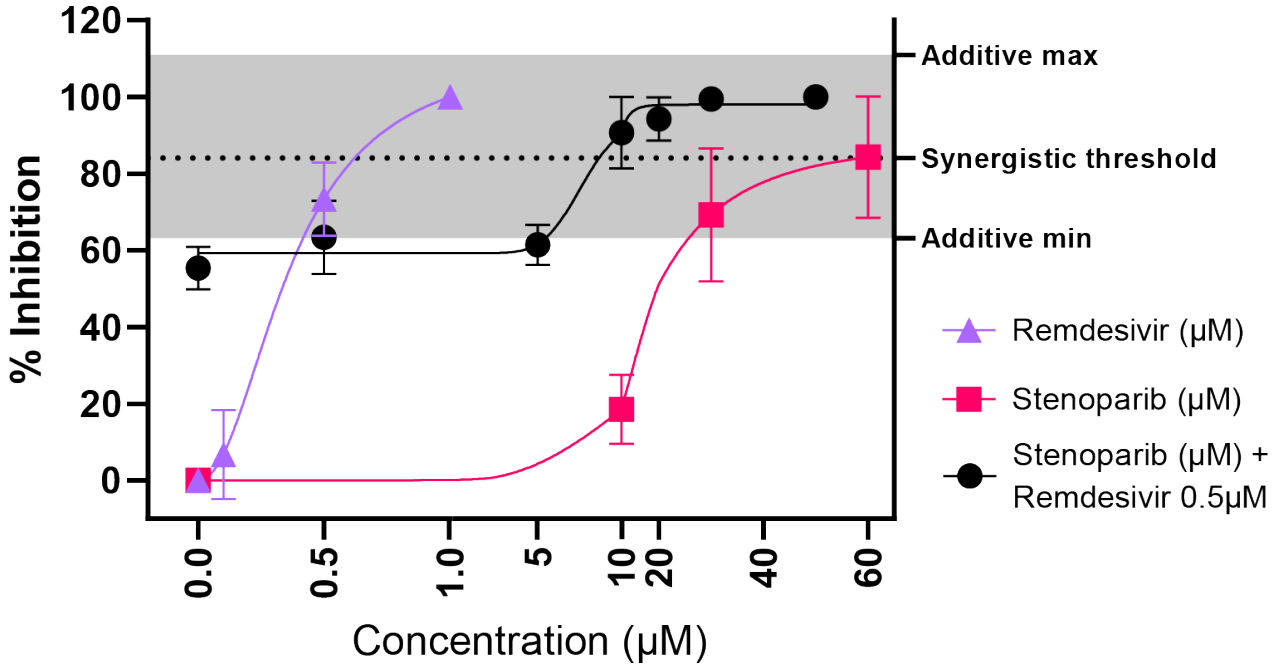
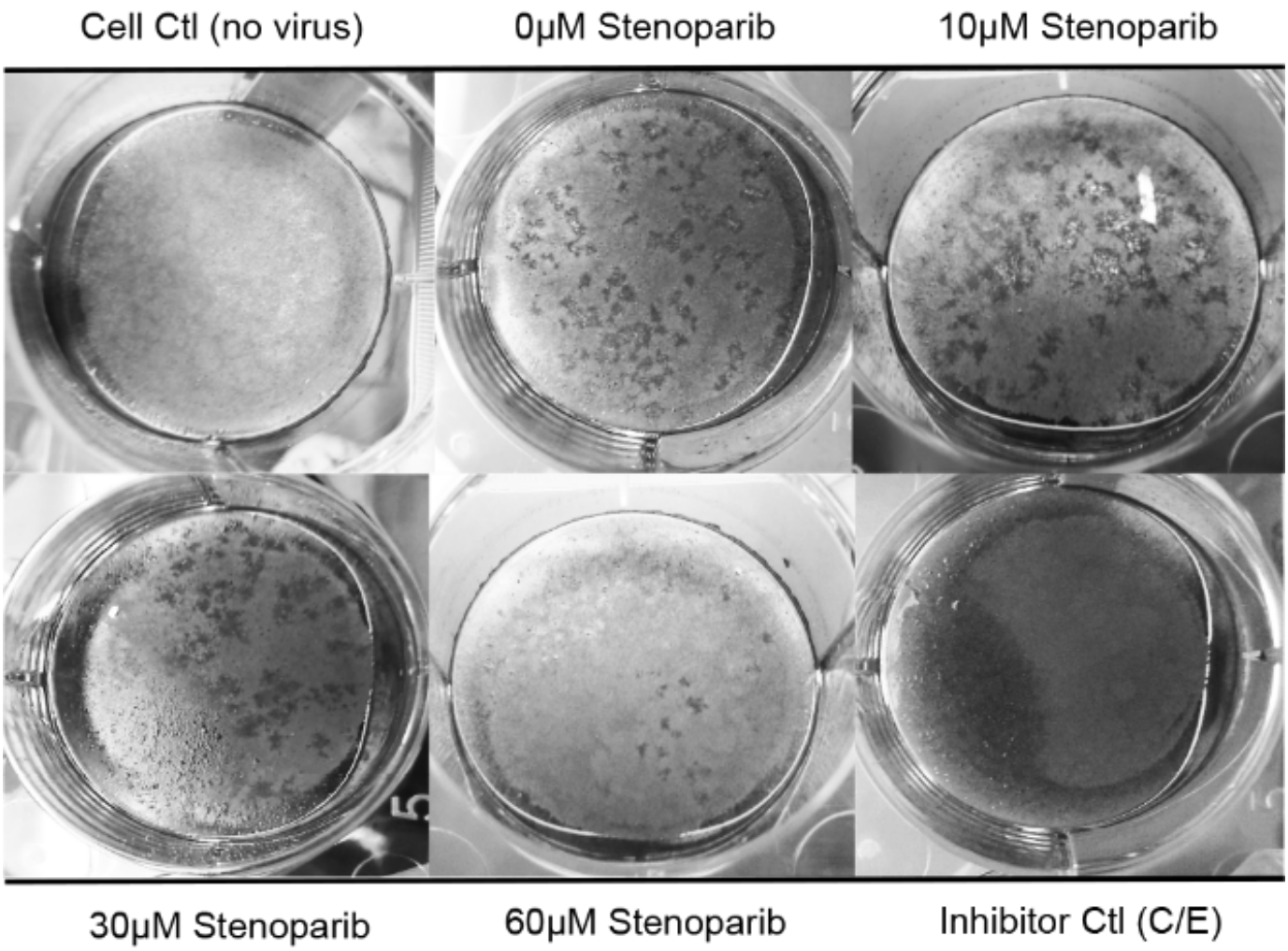
Fig. S1. Stenoparib inhibits plaque formation in Calu-3 cells. Plaque assays were performed using Calu-3 cells infected with SARS-CoV-2 and treated with varying concentrations of stenoparib. Plaques are identified as empty regions or "dead zones" in the cellular monolayer and are expressed as plaque forming units (PFUs) per well. Plaques were manually counted and averaged among experimental replicates. This score is normalized as a percentage of untreated, but infected cells. In this representative image of the SARS-CoV-2/Calu-3 experiment, plaques are dark scars on the cellular monolayer. Controls were 1) uninfected cells (Cell Ctl), 2) untreated, but infected cells (0 µM), and 3) a camostat mesylate and E64d (C/E) inhibitor control (Inhibitor Ctl). Treatment with stenoparib at 10 µM and 30 µM led to a marked reduction in plaquing efficiency, whereas 60 µM resulted in near complete inhibition.